Eng. Research Bull.
Faculty of Eng. & Tech.
Menoufia University
Vol. VI Part 1,1984
pp. 39 - 56

THEORETICAL INVESTIGATION OF FLUID FLOW THROUGH CURVED CHANNELS

E.A.SALEM[1] , *B.A.KHALIFA*[2] , *K.A.IBRAHIM*[3] , *A.A.KATAB*[4]

ABSTRACT

In the present study, a steady laminar of two dimension, isothermal and incompressible fluid flow through a curved channel of different curvature ratio has been studied theoretically,The governing equations of flow are derived in-terms of stream function and vorticity under the parabolic initial flow condition. A numerical solution, based on the finite difference method, is used to investigate the effects of Reynolds number, the angle of curved channel and the channel curvature ratio on the flow properties through curved channels. These properties, which are considered in this investigation, are; the axial velocity;the radial velocity; the pressure on the inner and outer walls; the pressure loss coefficient;the friction coefficient and flow separating point. The separating point was found to depend on the value of channel curvature ratio, it moves away in the upstream flow direction by increasing the value of curvature ratio.

1. *INTRODUCTION*

Fluid flow through curved pipes or channels has become of importance in a wide range of engineering applications, for example in the heating and cooling coils used in heat exchangers and refrigeration equipment. Curved conduit flows are encountered in many engineering problems, from heat exchangers to meandering rivers.

1 *Professor, Faculty of Eng. , Alexandria University.*
2 *Professor, Faculty of Eng. , Menoufia University.*
3 *Lecturer , Faculty of Eng. , Menoufia University.*
4 *Demonstrator, Faculty of Eng., Menoufia University.*

Unlike the case of straight channel, very little has been published concerned with theoretical and experimental studies of the flow through curved pipes or channels. ITO [1] made experimental study of fluid flow through smooth curved pipe of circular cross-section. He found that, for the case of turbulent flow, the static pressure at the outer wall has higher values than that at the inner wall and the pressure loss coefficient increases with the angle of curvature increases. Launder and Ying[2] studied the secondary flow in ducts of square cross-section. They showed that the ratio of secondary to primary velocity is greater in the case of rough duct than that for the case of smooth duct.

Yukimau, et. al[3] studied experimentally the hydraulic losses and the flow patters in the wavy and quasicoil bent pipes. Their results obtained may be summarized as follows; the hydraulic losses in the quasi-coil pipes composed of 90° bends and 90° screw type elbows are increased as the connecting angle increases. The losses in the wavy bent pipes are larger than those in quasi-coil pipes. Kulb and Seader [4]studied heat and mass transfer phenomena for viscous flow curved circular tubes. They showed that the friction losses of curved tubes are higher than those for the straight tubes. Mitsunobu and cheng[5] studied the laminar flow in the entrance region of curved parallel-plate channels. They showed that peak value of axial velocity moves away to the inner wall and also the radial pressure gradient has a higher value at the outer wall than that at the inner wall.

The main object of the theoretical work presented in this paper are; Determing the effects of Reynolds number, the angle of curved channel, and the channel

curvature ratio on the friction coefficient, pressure loss coefficient, the axial and radial velocities and the static pressure at both of the outer and inner walls. Also establishing a clear idea about the effect of channel curvature ratio on the flow separating point, for different values of flow Reynolds number.

NOMENCLATURE

a	: Normal distance from the center line of curved channel to the wall (half width of curved channel)
c_p	: Pressure loss coefficient = $\Delta P/\frac{1}{2}\rho V_m^2$.
D	: Curvature ratio $(a/\bar{R})$
f'	: Friction factor ratio $(f_c/f_s)=(\Delta P/\frac{1}{2}\rho V_m^2)$. $(2\ a/\bar{R}\ \theta)$
f_c	: Friction factor for the case of curved channel.
f_s	: Friction factor for the case of straight channel.
$\bar{P}$	: Static pressure
P	: Dimensionless pressure = $P/(\frac{1}{2}\rho V_m^2)$.
$\bar{R}$	: Curvature radius
$\bar{R}_1$	: Distance from the center of channel to any point on the width.
$\bar{R}+\bar{R}_1/a$	: Dimension-less radius, $(1 + D.R_1)/D$.
R_1	: Dimensionless distance, $R_1 = \bar{R}_1/a$.
R_e	: Reynolds number = $(V_m.2a)/\nu$.
$\bar{u}$, $\bar{v}$	: Velocity components in $\bar{R}_1$ and θ directions.
u, v	: Dimensionless velocity components in R_1 and θ directions $(\bar{u}.a/\nu\ ,\ \bar{v}/v_m)$.
$\bar{\bar{u}}$	: Radial velocity per mean axial velocity $(\bar{u}/v_m)$
V_m	: Axial mean velocity.
ρ	: Fluid density
ν	: Kinematic viscosity
θ	: Angle of curved channel
ψ	: Stream function
ζ	: Vorticity.

SUBSCRIPTS

I : Counter in radial direction
J : Counter in θ direction
N : Maximum counter in radial direction
0 : Initial condition
1 : Condition at any cross-section

2. *ANALYSIS*

The following assumptions apply to all the analytical work described below;

(1) The flow is steady, laminar, two-dimensional, isothermal and incompressible.
(2) The gravity forces are neglected compared to the other forces.
(3) The higher order of $\frac{\partial \psi}{\partial \theta}$ is neglected.

With the above assumptions and referring to Fig.(1), the basic equations governing the flow through curved channel are ;

Continuity equation

$$\frac{\partial \bar{u}}{\partial \bar{R}_1} + \frac{\bar{u}}{\bar{R} + \bar{R}_1} + \frac{1}{\bar{R} + \bar{R}_1} \frac{\partial \bar{V}}{\partial \theta} = 0 \qquad (1)$$

Momentum equation in $\bar{R}_1$ direction

$$u \frac{\partial \bar{u}}{\partial \bar{R}_1} + \frac{\bar{V}}{\bar{R}+\bar{R}_1} \cdot \frac{\partial \bar{u}}{\partial \theta} - \frac{\bar{V}^2}{\bar{R}+\bar{R}_1} = - \frac{1}{\rho} \frac{\partial \bar{P}}{\partial \bar{R}_1} + \nu \left[\frac{\partial^2 \bar{u}}{\partial \bar{R}_1^2} + \frac{1}{\bar{R}+\bar{R}_1} \cdot \frac{\partial \bar{u}}{\partial \bar{R}_1} - \frac{\bar{u}}{(\bar{R}+\bar{R}_1)^2} + \frac{1}{(\bar{R}+\bar{R}_1)^2} \cdot \frac{\partial^2 \bar{u}}{\partial \theta^2} - \frac{2}{(\bar{R}+\bar{R}_1)^2} \cdot \frac{\partial \bar{V}}{\partial \theta} \right] \qquad (2)$$

Momentum equation in θ direction .

$$\bar{u} \frac{\partial \bar{V}}{\partial \bar{R}_1} + \frac{\bar{V}}{\bar{R}+\bar{R}_1} \cdot \frac{\partial \bar{V}}{\partial \theta} + \frac{\bar{V} \cdot \bar{u}}{\bar{R}+\bar{R}_1} = - \frac{1}{\rho} \cdot \frac{1}{\bar{R}+\bar{R}_1} \cdot \frac{\partial \bar{P}}{\partial \theta} + \nu \left[\frac{\partial^2 \bar{V}}{\partial \bar{R}_1^2} + \frac{1}{\bar{R}+\bar{R}_1} \cdot \frac{\partial V}{\partial \bar{R}_1} + \frac{\bar{V}}{(\bar{R}+\bar{R}_1)^2} + \frac{1}{(\bar{R}+\bar{R}_1)^2} \cdot \frac{\partial^2 \bar{V}}{\partial \theta^2} + \frac{2}{(\bar{R}+\bar{R}_1)^2} \cdot \frac{\partial \bar{u}}{\partial \theta} \right] \qquad \ldots . (3)$$

Momentum equations, Equs(2) and (3) may be written in dimensionless form as follows;

Dimensionless momentum equation in $\bar{R}_1$ direction

$$u\frac{\partial u}{\partial R_1} + \frac{R_e.D}{2(1+D.R_1)}\cdot\frac{V\partial u}{\partial\theta} - \frac{R_e.D^2.V^2}{4(1+D.R_1)} - \frac{\partial^2 u}{\partial R_1^2} - \frac{D}{(1+D.R_1)}\cdot$$

$$\cdot\frac{\partial u}{\partial R_1} + \frac{D^2.u}{(1+D.R_1)^2} - \frac{D^2}{(1+D.R_1)^2}\cdot\frac{\partial^2 u}{\partial\theta^2} + \frac{R_e.D^2}{(1+D.R_1)^2}\cdot$$

$$\cdot\frac{\partial V}{\partial\theta} = -\frac{R_e^2}{8}\cdot\frac{\partial P}{\partial R_1} \qquad (4)$$

Dimensionless momentum equation in θ direction

$$\frac{1+D.R_1}{D}\cdot\frac{u\partial V}{\partial R_1} + \frac{R_e}{2}\cdot\frac{V\partial V}{\partial\theta} + u.v\frac{(1+D.R_1)}{D}\cdot\frac{\partial^2 V}{\partial R_1^2}$$

$$-\frac{\partial V}{\partial R_1} + \frac{D.V}{(1+D.R_1)} - \frac{D}{(1+D.R_1)}\cdot\frac{\partial^2 V}{\partial\theta^2} - \frac{4D}{R_e(1+D.R_1)}\cdot$$

$$\cdot\frac{\partial u}{\partial\theta} = -\frac{R_e}{4}\cdot\frac{\partial P}{\partial\theta} \qquad (5)$$

where, the dimensionless parameters; R_1; V; u; P; D and R_e are defined in the nomenclature.

The dimensionless velocity components u and v may be calculated from the following relations ;

$$v = \frac{\partial\psi}{\partial R_1} \qquad (6)$$

$$u = -\frac{D}{(1+D.R_1)}\cdot\frac{\partial\psi}{\partial\theta} \qquad (7)$$

while the radial velocity per mean axial velocity was calculated from the following relation;

$$\bar{u} = -\frac{2}{R_e}\cdot\frac{D}{(1+D.R_1)}\cdot\frac{\partial\psi}{\partial\theta} \qquad (8)$$

Using Equs(6) and (7) in the Equs(4) and (5), and after eliminating the pressure term, the following equation of motion may be obtained ;

$$\nabla^2 \zeta = \frac{R_e . D}{2(1+D.R_1)} \left(\frac{\partial \psi}{\partial R_1} . \frac{\partial}{\partial \theta} - \frac{2}{R_e} . \frac{\partial \psi}{\partial \theta} . \frac{\partial}{\partial R_1} \right) . \zeta \qquad (9)$$

where ;

$$\zeta = \nabla^2 \psi$$

and

$$\nabla^2 = \frac{\partial^2}{\partial R_1^2} + \frac{D}{1+D.R_1} . \frac{\partial}{\partial R_1} \qquad (10)$$

In order to predict the pressure loss and friction ratio coefficients, the following equations, [5]. were used ;

$$C_p = \frac{P_o - \bar{P}_1}{\frac{1}{2} \rho V_m^2} \qquad (11)$$

$$f' = \frac{P_o - \bar{P}_1}{\frac{1}{2} \rho V_m^2} . \frac{2 a}{\bar{R} . \theta} \qquad (12)$$

In Eq(11) $\bar{P}_1$ is the average pressure over any cross section of the channel.

$$\bar{P}_1 = \int_{\bar{R}_1=-a}^{\bar{R}_1=a} \bar{P} . \bar{R}_1 . d\bar{R}_1 \Big/ \int_{\bar{R}_1=-a}^{\bar{R}_1=a} \bar{R}_1 . d\bar{R}_1 \qquad (13)$$

By using the finite difference approximations and the Crank-Nicolson method, Eqs(4, 5, 6, 8, 9 and 10) are converted into the following simultaneous linear equation;

$$- \frac{R_e}{8} . \frac{P_{(I+1,J+1)} - P_{(I,J+1)}}{\Delta R_1} = C_1 + \frac{R_e}{2.R_{(I)}} . C_2 - \frac{R_e^2}{4.R_{(I)}} . V^2_{(I,J+1)} - C_3 - \frac{C_4}{R_{(I)}} - \frac{U_{(1,J+1)}}{R^2_{(I)}} - \frac{C_5}{R^2_{(I)}} + \frac{R_e . C_6}{R^2_{(I)}} \qquad (\bar{4})$$

$$- \frac{R_e}{4} . \frac{P_{(I,J+1)} - P_{(I,J)}}{\Delta \theta} = C_7 + \frac{R_e}{2} . C_8 + C_9 - R_{(I)} . C_{10} - C_{11} + \frac{V_{(I,J+1)}}{R_{(I)}} - \frac{C_{12}}{R_{(I)}} - \frac{4 . C_{13}}{R_e . R_{(I)}} \qquad (\bar{5})$$

$$V_{(I,J+1)} = \frac{\psi_{(I+1,J+1)} - \psi_{(I-1,J+1)}}{2.\ \Delta R_1} \qquad (\bar{6})$$

$$\bar{\bar{U}}_{(I,J+1)} = \frac{-2}{R_e \cdot R_{(I)}} \cdot \frac{\psi_{(I,J+1)} - \psi_{(I,J)}}{\Delta\ \theta} \qquad (\bar{8})$$

$$\frac{R_e}{2R_{(I)}} \cdot \frac{\zeta_{(I,J+1)} - \zeta_{(I,J)}}{\Delta\ \theta} = C_{14} + C_{15} + C_{16} \qquad (\bar{9})$$

$$\zeta_{(I,J+1)} = C_{17} + C_{18} \qquad (\bar{10})$$

where

$$C_1 = U_{(I,J)} \cdot \frac{U_{(I,J+1)} - U_{(I-1,J+1)}}{\Delta R_1} \cdot$$

$$C_2 = V_{(I,J)} \cdot \frac{U_{(I,J+1)} - U_{(I,J)}}{\Delta\ \theta}$$

$$C_3 = \frac{U_{(I+1,J+1)} - 2U_{(I,J+1)} + U_{(I-1,J+1)}}{\Delta R_1^2}$$

$$C_4 = \frac{U_{(I+1,J+1)} - U_{(I,J+1)}}{\Delta R_1}$$

$$C_5 = \frac{U_{(I,J+1)} - 2U_{(I,J)} + U_{(I,J-1)}}{\Delta\ \theta^2}$$

$$C_6 = \frac{V_{(I,J+1)} - V_{(I,J)}}{\Delta\ \theta}$$

$$C_7 = R_{(I)} \cdot U_{(I,J)} \cdot \frac{V_{(I+1,J+1)} - V_{(I-1,J+1)}}{2\ .\ \Delta\ R_1}$$

$$C_8 = V_{(I,J)} \cdot \frac{V_{(I,J+1)} - V_{(I,J)}}{\Delta\ \theta}$$

$$C_9 = U_{(I,J)} \cdot V_{(I,J+1)}$$

$$C_{10} = \frac{V_{(I+2,J+1)} - 2V_{(I+1,J+1)} + V_{(I,J+1)}}{\Delta R_1^2}$$

$$C_{11} = \frac{V_{(I+1,J+1)} - V_{(I,J+1)}}{\Delta R_1}$$

$$C_{12} = \frac{V_{(I,J+1)} - 2V_{(I,J)} + V_{(I,J-1)}}{\Delta\ \theta^2}$$

$$C_{13} = \frac{U_{(I,J+1)} - U_{(I,J)}}{\Delta\theta}$$

$$C_{14} = \frac{\zeta_{(I+1,J+1)} - 2\zeta_{(I,J+1)} + \zeta_{(I-1,J+1)} - \zeta_{(I+1,J)} + 2\zeta_{(I,J)}}{2\,\Delta R_1^2} -$$

$$- \frac{\zeta_{(I-1,J)}}{2\,\Delta R_1^2}$$

$$C_{15} = \frac{1}{R_{(I)}} \cdot \frac{\zeta_{(I+1,J+1)} - \zeta_{(I-1,J+1)} - \zeta_{(I+1,J)} + \zeta_{(I-1,J)}}{4 \cdot \Delta R_1}$$

$$C_{16} = U_{(I,J)} \cdot \frac{\zeta_{(I+1,J+1)} - \zeta_{(I-1,J+1)} - \zeta_{(I+1,J)} + \zeta_{(I-1,J)}}{4 \cdot \Delta R_1}$$

$$C_{17} = \frac{\psi_{(I+1,J+1)} - 2\psi_{(I,J+1)} - \psi_{(I-1,J+1)}}{2\,\Delta R_1^2} -$$

$$- \frac{\psi_{(I+1,J)} - 2\psi_{(I,J)} + \psi_{(I-1,J+1)}}{2\,\Delta R_1^2}$$

$$C_{18} = \frac{1}{R_{(I)}} \cdot \frac{\psi_{(I+1,J+1)} - \psi_{(I-1,J+1)}}{4 \cdot \Delta R_1} - \frac{\psi_{(I+1,J)} - \psi_{(I-1,J)}}{4 \cdot \Delta R_1}$$

The value of axial velocity at any point of channel cross section may be obtained from Eq($\bar{6}$). While the values of radial velocities at points (I =1,2,..N) were obtained from Eq($\bar{8}$). After obtaining all values of axial velocity, the accuracy of the numerical technique was obtained from the following relation;

$$\text{Error} = \frac{Q_{(J)} - Q_{(J+1)}}{Q_{(J)}} \leq 10^{-4}$$

where; $Q_{(J)}$ is discharge at section (J) and $Q_{(J+1)}$ is the discharge at section (J+1).

The dimensionless static pressure distribution, at the inner wall (I=1,J=J) and at the outer wall (I=N+1,J=J), was calculated from the linearized finite difference Eqs ($\bar{4}$ and $\bar{5}$).

The calculation procedure and the computer program used to solve these equations are given in [6]. In the calculations,the following boundary and initial flow conditions are used; at the inner and outer walls the velocities are equal zero, $\psi = -1$ at the inner wall and $\psi = 1$ at the outer wall. While at $\theta = 0$, the following conditions are used;

$$V = 3\ (1 - R_1^2)/2$$

$$\psi = R_1 \cdot (R_1^2 - 3)/2$$

$$\zeta = -3\ R_1 - 3\ (R_1^2 - 1)/2R$$

$$u = 0$$

$$P = P_o$$

3. *RESULTS AND DISCUSSION*

3.1. *Axial velocity distribution*

A representative selection of the axial velocity profiles, for different values of θ are shown in Fig. (2). From this figure it can be seen that the axial velocity decreases in the inner half of channel by increasing the angle (θ), while the axial velocities in the outer half of channel are increasing by increasing the angle (θ). This is due to the centrifugal forces which occur in the flow. By increasing the angle θ, the flow starts to separate on the inner wall, as shown in Fig.(1). This point of flow separation was found to depend on the value of channel curvature ratio (D); it moves a way in the upstream flow direction by increasing the value of (D), see Fig.(3). The peak values of axial velocities, which occur in the outer half of channel, have higher values for the case of higher curvature ratio than those for the case of smaller D. This is because the centrigugal

forces are increasing by increasing the value of (D). From the results illustrated in Figs(3 and 4) for R_e = 500 and 2500, it can be seen that the axial velocity profiles are similar in their trend and the effect of R_e on the axial velocity is not quite clear. This is because the initial flow velocity was considered as the mean value of axial flow velocity.

3.2. Radial velocity distribution

The radial velocities distributions at different sections are shown in Fig.(5). From this figure it can be seen that, at constant values of R_e and D, the radial velocity $\bar{\bar{u}}$ decreases by increasing the angle θ. The absolute value of this velocity in the inner half of channel is higher than that in the outer half of channel. This is due to the decay of axial velocity in the inner half of channel. The effect of changing the value of D on the variation of radial velocity is quite clear in Fig.(6). The radial velocity increases with D increases and the peak value of $\bar{\bar{u}}$ moves to the origin by decreasing the value of D. Concerning the effect of R_e on the $\bar{\bar{u}}$, the results for different values of R_e are shown in Fig.(7).The radial velocity decreases by increasing the value of R_e as shown in Fig.(7). This can be explained according to Equ(8), if R_e increases the value of $\bar{\bar{u}}$ decreases.

3.3. Pressure distribution

The results of dimensionless pressure distribution at the inner and outer walls for different values of D and R_e are shown in Figs(8, 9 and 10). It is noticed, from these figures, that the pressure at the inner and outer walls for any angle θ increases

by increasing the curvature ratio. The effect of changing the angle (θ) on the variation of pressure is also clear in these figures; where the value of pressure decreases with (θ) increases, for all values of D and R_e tested here. The effect of changing the value of R_e on the dimensionless pressure distribution at the inner and outer walls is also clear in Figs(9 and 10). From these figures it can be seen that the variation of pressure along the curved channel increases by increasing the R_e. This is because the inertia forces are larger than the viscous forces for the case of increasing the value of R_e. From Fig. (8) it can be seen that the pressure at the outer wall(P_{oi}) has a higher value than the pressure at the inner wall along the curved channel. But the variation of pressure difference between the outer and the inner walls is small because the surface length of the outer wall is longer than the length of the inner surface. This variation increases by increasing the value of(D).

3.4. Pressure loss coefficient

The variation of pressure loss coefficient (C_p) with the angle of curved channel (θ) at different values of D and R_e is illustrated in Figs (11 and 12). At any value of θ, the value of C_p decreases by increasing the curvature ratio; see Fig.(11). This is due to the decrease in the value of pressure drop by increasing the curvature ratio (D) as was discussed in subsection 3.3. Concerning the effect of R_e on the variation of C_p, the calculations were made for different values of R_e and the results are illustrated in Fig.(12). From this figure it can be noticed that, at constant value of θ and D,$C_p$decreases by increasing the value of R_e. Also from this figure it can be seen

that the value of C_p increases sharply by increasing the value of θ, for all values of R_e.While for(D>0.3). the rate of increase of C_p is slightly small, see Fig. (11).

3.5. Friction coefficient ratio

The friction coefficient ratio (f')was calculated at different values of D, R_e and θ. The results are illustrated in Figs(13 - 15).From these figures it is noticed that, the value of f' decreases with the angle θ increases for all tested values of D and R_e. The friction factor f' decreases by increasing (D), see Fig.(13).The value of f' is equal to zero at separating flow point, which moves back in the upstream flow direction by increasing the value of D. This is due to the increasing value of centrifugal forces by increasing the value of D. For D = 0.1 the separation flow phenomenon does not occur along the inner surface of curved channel, which is assumed here to have angle of curvature of 30°, see Figs(13 and 14). But for D = 0.3, the flow separates at θ= 22.8°, and for D = 0.5, the flow separates at θ= 13.8°. While for D = 0.7, the flow separates at θ= 10.8°. From these figures it can be concluded that, the separating point in curved channels depends on the value of curvature ratio of these channels. While the Reynolds number has no significant effect on the separation flow phenomenon through curved channels see Fig. (15). This may be connected with the assumed initial flow condition, which indirectly includes the R_e.

4. CONCLUSIONS

The behaviour of fluid flow through curved channels with different angles of curvature was stuided numerically. From the theoretical analysis given in this study, the following conclusions may be drawn :

(a) The general flow equations for fluid flow through a curved channel are derived in terms of angle of curvature, curvature ratio and the Reynolds number. The equations are formulated in the finite difference form.

(b) The variation of inner pressure, outer pressure, axial velocity, radial velocity, pressure loss coefficient, friction coefficient ratio in curved channel has been shown to depend significantly on the angle of curvature, the curvature ratio and the Reynolds number.

(c) The separating flow point was found to depend on the value of channel curvature ratio; it moves back in the upstream flow direction by increasing the value of curvature ratio. For example, if fluid flows through a 30° curved channel, the flow does not separate at curvature ratio = 0.1. But it separates at curvature ratio greater than 0.1 as follows ;

   i) At curvature ratio = 0.3, the flow separates at θ= 22.8°.

   ii) At curvature ratio = 0.5, the flow separates at θ= 13.8°.

   iii) At curvature ratio = 0.7, the flow separates at θ= 10.8°.

REFERENCES

1] Ito, H, "Pressure losses in smooth Pipe bends ", Trans. ASME, series D, J. Basic Eng., P. 131, 1960.

2] Launder, B.E. and Ying, W.M., "Secondary flow in ducts of square cross-section", J. Fluid Mech, Vol. 54, Part 2, p. 289, 1972.

3] Yukimaru, S., Koichi, S., Sadao, K. and Mitsukiyo, M., "Hydraulic losses and flow Patterns in bend pipes (comparison of the results in wavy pipes and qussi-coiled ones)", Bull. of JSME, Vol. 25, No.199, 1982.

4] Kalb, C.E. and Seader, J.D., "Heat and mass transfer Phenomena for viscous flow in curved circular tubes",J.Heat mass transfer, Vol.15, P. 801, 1971.

5] Mitsunobu, A. and Cheng, K.C., "Laminar flow in the entrance region of curved parallel plate channels", J.App. Mech.,P.463, 1976.

6] Khatab, A.A., "Fluid flow in curved pipes", M. Sc. thesis, Mech. Eng. Dept., Menoufia University, 1984.

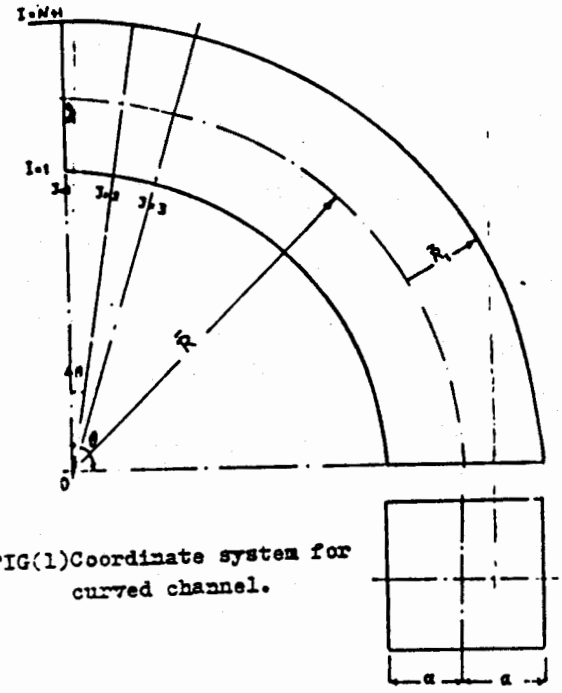

FIG(1)Coordinate system for curved channel.

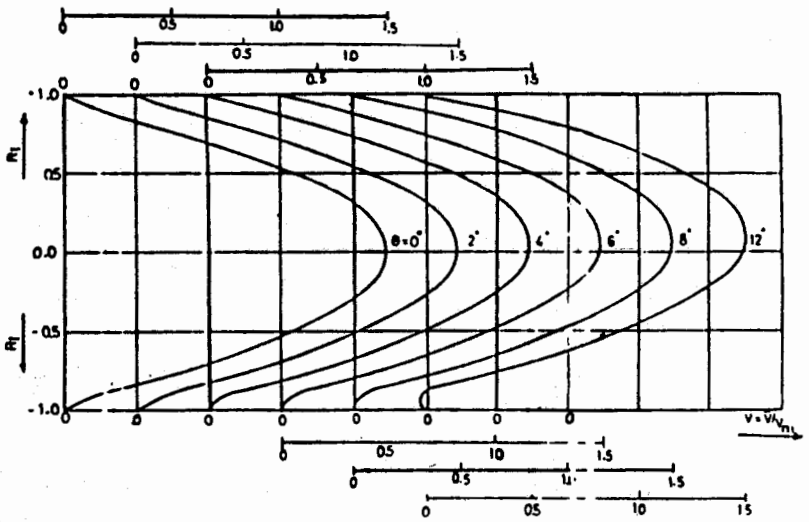

FIG(2)Dimensionless axial velocity distribution across channel cross-section(D=0.7),R_e=500

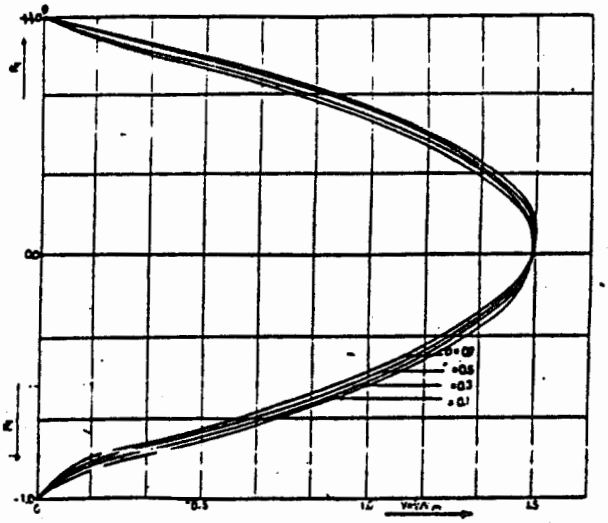

IG(3)Dimensionless axial velocity distribution across channel cross-section(R_e=500),θ=8°

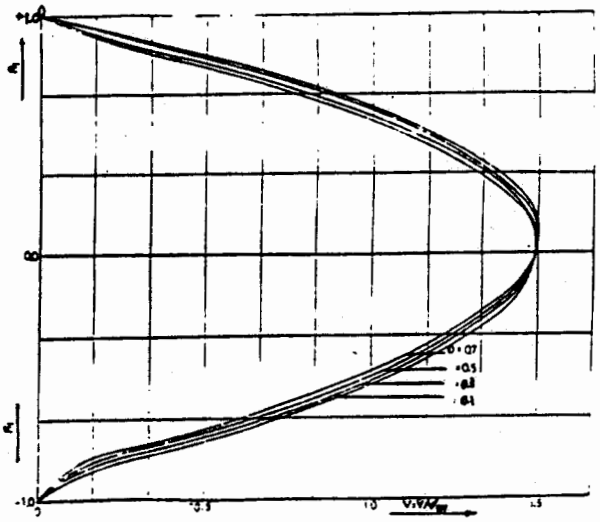

FIG(4)Dimensionless axial velocity distribution across channel cross-section(R_e=2500),θ=8°

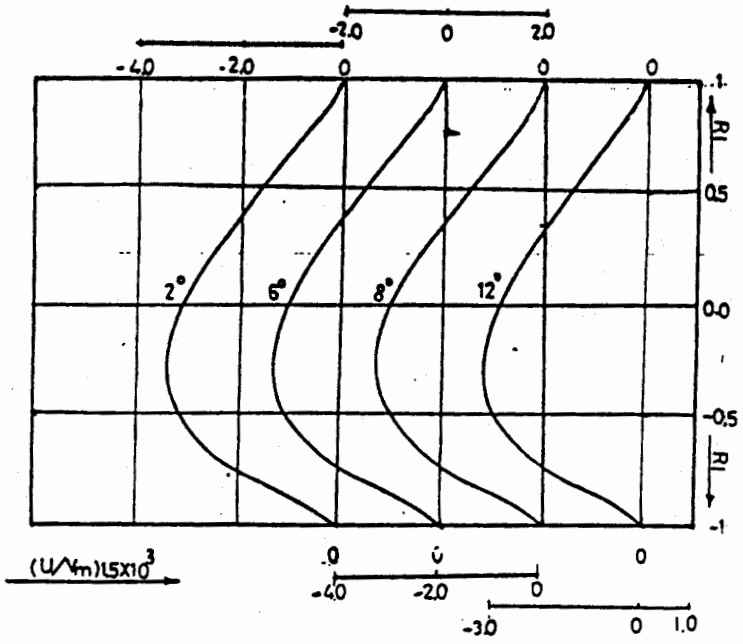

Fig(5)Dimensionless radial velocity distribution across channel cross-section (D=0.7 R_e=500)

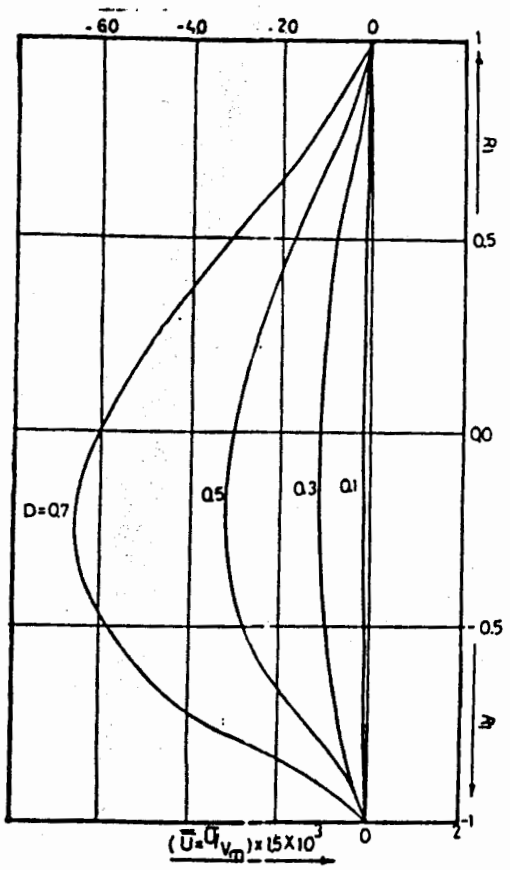

FIG(6)Dimensionless radial velocity distribution across channel cross-section(θ=8° R_e=500)

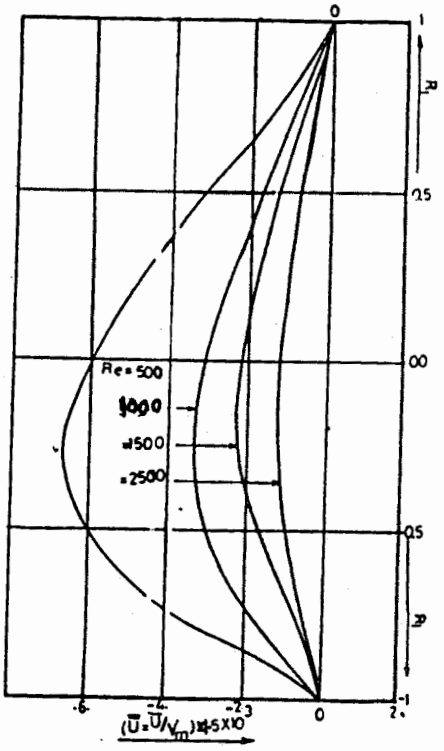

FIG(7)Dimensionless radial velocity distribution across channel cross-section(θ=8°, D=0.7)

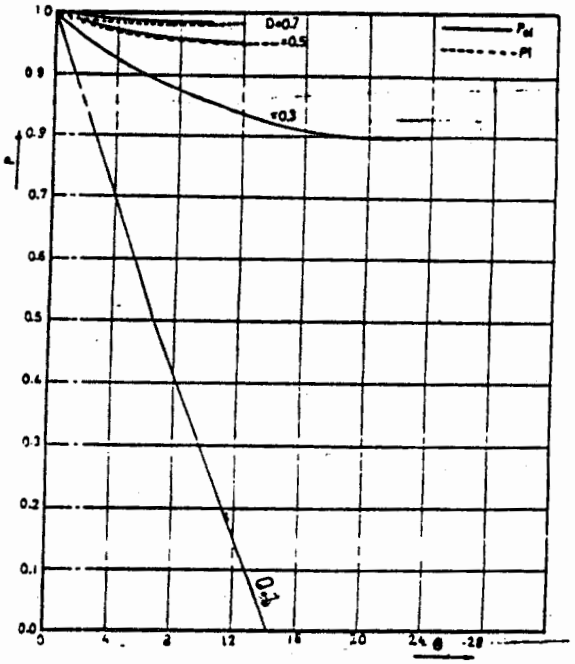

FIG(8)Variation of static pressure on the inner and outer walls with the angle θ,(R_e=500)

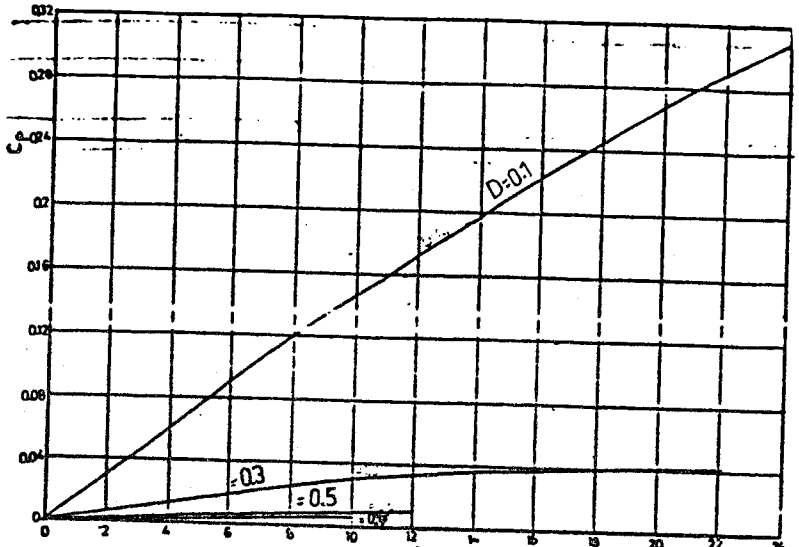

FIG(11)Variation of pressure loss coefficient with the angle(θ),(R_e=2500)

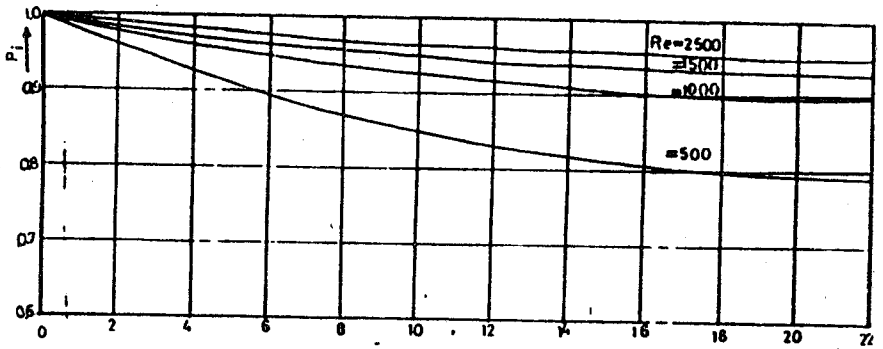

FIG(9)Variation of dimensionless static pressure on the inner wall with the angle of curvature(θ),(D=0.3)

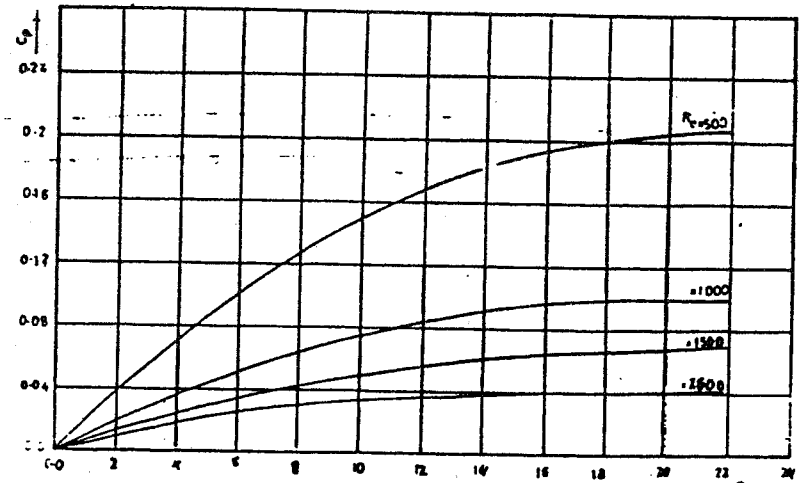

FIG(12)Variation of pressure loss coefficient with the angle(θ),(D=0.3)

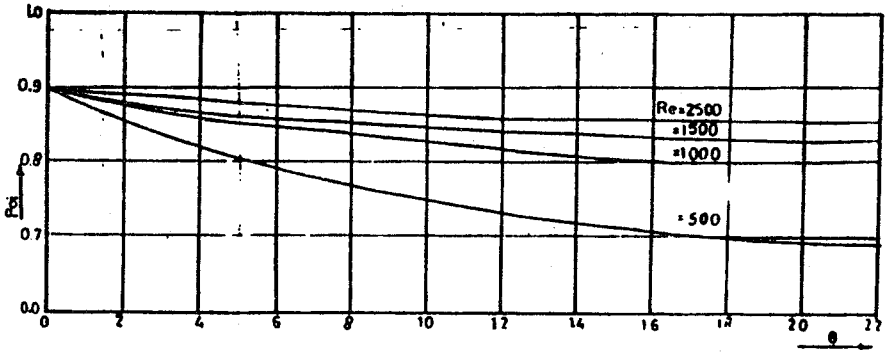

FIG(10)Variation of dimensionless static pressure of the outer wall with the angle of curvature(θ),(D=0.3)

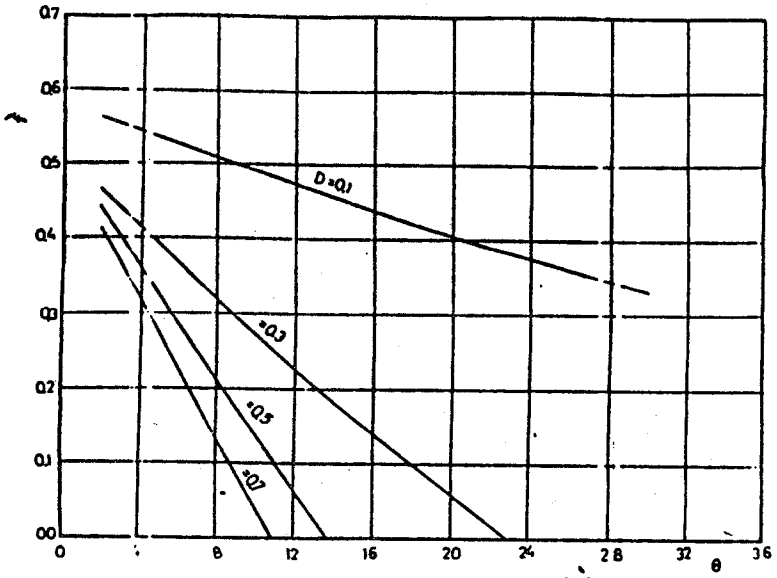

FIG(13)Variation of friction factor ratio($\bar{F}$) with the angle of(θ),(R_e=1000)

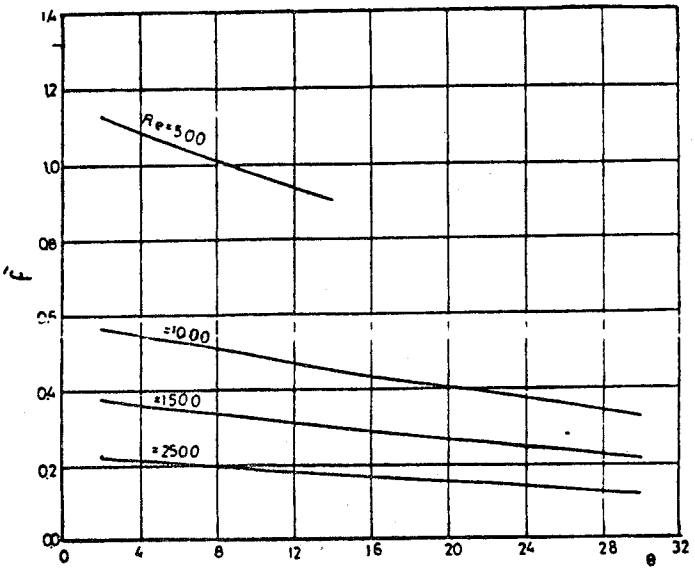

FIG(14)Variation of friction factor ratio($\bar{F}$) with the angle(θ),(D=0.1)

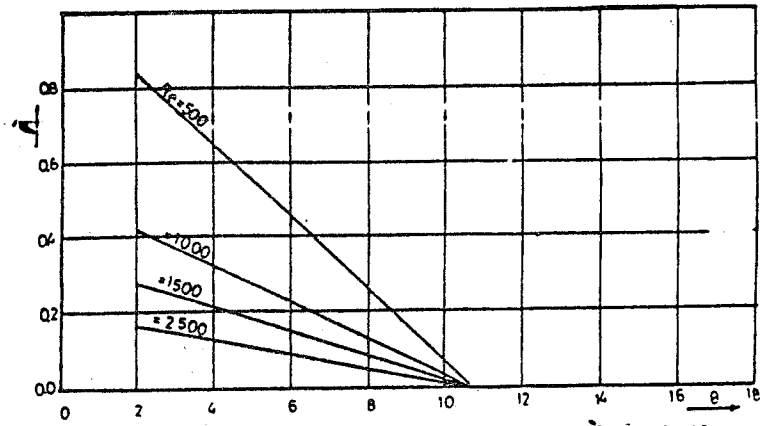

FIG(15)Variation of friction factor ratio($\bar{F}$) with the angle(θ),(D=0.7)